Hindawi
Journal of Nanomaterials
Volume 2017, Article ID 3108586, 9 pages
https://doi.org/10.1155/2017/3108586

Research Article

Physical Background for Luminescence Thermometry Sensors Based on Pr^{3+}:LaF_3 Crystalline Particles

Maksim S. Pudovkin,[1] Oleg A. Morozov,[1] Vitaly V. Pavlov,[1] Stella L. Korableva,[1] Elena V. Lukinova,[1] Yury N. Osin,[1] Vladimir G. Evtugyn,[1] Roman A. Safiullin,[2] and Vadim V. Semashko[1]

[1]*Kazan Federal University, Kazan, Tatarstan 420008, Russia*
[2]*Kazan National Research Technological University, Kazan, Tatarstan 420015, Russia*

Correspondence should be addressed to Maksim S. Pudovkin; jaz7778@list.ru

Received 12 May 2017; Revised 31 July 2017; Accepted 15 August 2017; Published 24 September 2017

Academic Editor: Victor M. Castaño

The main goal of this study was creating multifunctional nanoparticles based on rare-earth doped LaF_3 nanocrystals, which can be used as fluorescence thermal sensors operating over the 80–320 K temperature range including physiological temperature range (10–50°C). The Pr^{3+}:LaF_3 (C_{Pr} = 1%) microcrystalline powder and the Pr^{3+}:LaF_3 (C_{Pr} = 12%, 20%) nanoparticles were studied. It was proved that all the samples were capable of thermal sensing into the temperature range from 80 to 320 K. It was revealed that the mechanisms of temperature sensitivity for the microcrystalline powder and the nanoparticles are different. In the powder, the $^3P_1$ and $^3P_0$ states of Pr^{3+} ion share their electronic populations according to the Boltzmann and thermalization of the $^3P_1$ state takes place. In the nanoparticles, two temperature dependent mechanisms were suggested: energy migration within $^3P_0$ state in the temperature range from 80 K to 200 K followed by quenching of $^3P_0$ state by OH groups at higher temperatures. The values of the relative sensitivities for the Pr^{3+}:LaF_3 (C_{Pr} = 1%) microcrystalline powder and the Pr^{3+}:LaF_3 (C_{Pr} = 12%, 20%) nanoparticles into the physiological temperature range (at 45°C) were 1, 0.5, and 0.3%°C^{-1}, respectively.

1. Introduction

Nanothermometry aims to measure the local temperature of a studied system with submicrometric spatial resolution [1]. Among different thermometers such as nanoscale thermocouples [2] and coulomb blockade nanothermometers [3], the luminescent nanothermometers hold a special place because of its high spatial and temporal resolution, accuracy, and contactlessness [1, 4–6]. The luminescent nanothermometry is based on the luminescence features which are analyzed and which are used for the temperature measurement [1, 4]. Luminescent nanothermometers are widely applied in the thermal imaging of integrated circuits [7], in vitro and in vivo imagining of biological objects [8], the subtissue thermal sensing [9–11], and temperature detecting for harsh environments or fast moving objects [12]. Generally, there are six parameters that define the luminescence emission of a material: intensity, lifetime, band shape, band width, polarization, and spectral position [1]. Therefore, the luminescent nanothermometers can be grouped into six corresponding subclasses. The most widespread is the subclass of luminescent nanothermometers based on the analysis of relative fluorescence intensity between the different emission bands corresponding to the suitable transitions [1, 9, 13]. Among the most usable materials for luminescent nanothermometers such as quantum dots (QD) and dye-based luminescent nanothermometers, the rare-earth based materials have a special place mainly because of their excellent photostability, long luminescent lifetimes, sharp emission bands, and low toxicity which is highly important for biomedical application, for example, in photothermal and photodynamic therapies [14]. Indeed, in biomedicine, the luminescent nanothermometers should be nontoxic and stay chemically stable under light irradiation so that toxic components of reaction product

are not delivered to the cells [1]. Generally, toxicity of inorganic substances generally depends on their solubility in the water. Also rare-earth doped fluorides demonstrate the lowest solubility among other rare-earth based materials (oxides et al.). For instance, the CeF_3 and other trifluorides with tysonite crystal structure demonstrate solubility around 10^{-5}–10^{-6} mol/L. and as a consequence low toxicity [15]. The lanthanides such as Dy^{3+}, Er^{3+}, Nd^{3+}, Yb^{3+}, Sm^{3+}, and Pr^{3+} demonstrate temperature sensitivity in different temperature ranges providing different absolute (K^{-1} or $^{\circ}C^{-1}$) and relative ($\%K^{-1}$ or $\%^{\circ}C^{-1}$) sensitivities. In general, for the majority of lanthanides, temperature sensing technique is based on the ratio of the fluorescence intensity of the emission bands corresponding to the suitable transitions [1]. For example, Dy^{3+}:LaF_3 glass ceramics under 352 nm excitation ($^6P_{7/2}$ of Dy^{3+}) demonstrate sensitivity $1.16 * 10^{-4}\,K^{-1}$ obtained at T = 294 K [6] and the temperature is extracted from the ratio of the fluorescence intensities of the 480 and 572 nm emission bands corresponding to $^4F_{9/2}$-$^6H_{15/2}$ and $^4F_{9/2}$-$^6H_{13/2}$ transitions of Dy^{3+} [6]. For such ions as Pr^{3+} and Er^{3+} the same approach is used and these ions operate in overlapping temperature ranges of 300–600 K and 300–2000 K, respectively [12, 16]. For the biomedical applications and in vitro and in vivo experiments, the luminescent thermometers which can operate in physiological temperature range (10–60°C) are highly relevant [9]. Sm^{3+}:TiO_2 NPs operating in a temperature range from room temperature to 110°C demonstrate that maximum value of relative sensitivity is $10.54\%^{\circ}C^{-1}$ at 57.5°C [17]. The Nd^{3+} based luminescent nanothermometers such as Nd^{3+}:LaF_3 NPs or active-core/active-shell Nd^{3+}- and Yb^{3+}-doped LaF_3 NPs are exited at 808 nm wavelength which lays in the biological window (650–1350 nm) what paves the way toward subcutaneous thermal sensing [9–11, 18]. For example, the active-core/active-shell Nd^{3+}/Yb^{3+}-doped LaF_3 NPs demonstrate relative thermal sensitivity around $0.41 \pm 0.01\% \cdot {}^{\circ}C^{-1}$, at 10°C [9, 11]. The systems based on Pr^{3+} are studied in [19–21]. In case of Pr^{3+} ions, the energy gap between $^3P_0$ and the next-highest state, $^3P_1$, is only a few hundred cm^{-1} for most host matrixes (for example, for LaF_3 [22] and $CsCdBr_3$ [22] it is around 500 cm^{-1}), $^3P_1$ becomes thermally populated following $^3P_0$ excitation, and the luminescence spectrum contains both $^3P_0$ and $^3P_1$ emission, with intensity ratios consistent with the predicted Boltzmann distribution among these states [22]. In particular, in [19], the temperature sensing technique is based on the ratio of the fluorescence intensity for $^3P_1 \rightarrow {}^3H_5$ and $^3P_0 \rightarrow {}^3H_5$ transitions in temperature range 273–453 K providing sensitivity within ~$1.15\%K^{-1}$. Also, Pr^{3+} demonstrates strong luminescence lifetime dependence on temperature as it is shown in [21]. For the system Pr^{3+}:YAG the measured lifetime of $^1D_2$ decreases linearly from ~190 μs at 0°C to ~110 μs at 1000°C. From another side, the thermal sensing materials based on Pr^{3+} ions attract great attention of the scientific community because of its thermal sensitivity in broad temperature range [12, 23] and biomedical potential [24].

Also it should be noted that during the last two decades, an immense progress has been done toward facile synthesis of LnF_3 nanoparticles (NPs) with different size and shape [25, 26]. For these reasons, LaF_3 host matrix is considered as a very promising material for doping with rare-earth elements for broad range of applications.

Here we analyze the temperature dependent luminescence features of Pr^{3+} doped LaF_3 both microcrystalline powder and crystalline NPs and demonstrate the opportunity of applying them as nanothermometers for the 80–320 K temperature range, especially focusing on the physiological one (10–60°C).

2. Materials and Methods

2.1. Growth of the Pr^{3+}:LaF_3 (C_{Pr} = 1%) Crystal, Synthesis of the Pr^{3+}:LaF_3 (C_{Pr} = 12%, 20%) Nanoparticles, and Their Characterization. All the samples were obtained in the MRS laboratory, Institute of Physics, Kazan Federal University.

The NPs Pr^{3+}:LaF_3 (C_{Pr} = 20%) were synthesized via coprecipitation method. 0.4 g Pr_2O_3 and 2 g La_2O_3 were added to 110 mL of 10% nitric acid in a polypropylene glass. The mixture was heated to 50°C and stirred for 45 min; then a transparent light-green solution appeared. Then the mixture was filtered and placed in an ultrasonic cleaner (ultrasonic power 100 W) and solution of 3 g of NaF in 100 mL of distillated water was added. Then the pH was adjusted to 4 by adding 25% solution of ammonium hydrate. Then the mixture was stirred for 10 minutes under the ultrasonic treatment. The precipitation was purified with distillated water by centrifugation (12,000 revolutions/min, centrifugation time 15 min) for 8 times. The presence of nitrates after each stage of centrifugation was controlled via diphenylamine test. In order to synthesize Pr^{3+}:LaF_3 (C_{Pr} = 12%) NPs, the suitable ratio of Pr_2O_3 and La_2O_3 was taken. Then nanoparticles were dried in air. The structure of the material was characterized by X-ray diffraction method with Shimadzu XRD-7000S X-ray diffractometer. Analysis of samples was carried out in a transmission electron microscope Hitachi HT7700 Exalens. Sample preparation was followed: 10 microliters of the suspension was placed on a formvar/carbon lacey 3 mm copper grid; drying was performed at room temperature. After drying, grid was placed in a transmission electron microscope using special holder for microanalysis. Analysis was held at an accelerating voltage of 100 kV in TEM mode. The control of amount of nitrates in colloidal solution of the NPs after each stage of centrifugation was performed by identification test using diphenylamine (diphenylamine test).

The Pr^{3+}:LaF_3 (C_{Pr} = 1%) crystal was grown by the method of directional solidification in graphite crucibles [27]. The samples were cylinder shape of 6 mm diameter and 20 mm length. The microcrystalline powder was obtained by mealing.

The luminescence spectra were recorded using CCD spectrometer (StellarNet), which detects the emission in 200–1100 nm spectral range with a spectral resolution of 0.5 nm. The optical parametric oscillator laser system (420–1200 nm) from JV LOTIS TII was used for excitation

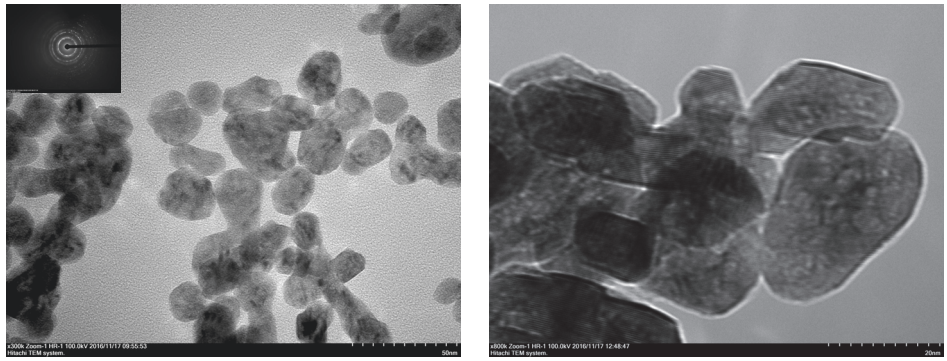

(a) (b)

Figure 1: (a) TEM images and SAED patterns of the Pr^{3+}:LaF_3 (C_{Pr} = 12%) nanoparticles. (b) TEM image of the lattice structures of the Pr^{3+}:LaF_3 (C_{Pr} = 12%) nanoparticles under the higher magnification.

of the luminescence of the samples. The pulse width and the pulse-repetition rate were 10 ns and 10 Hz, respectively. The spectral width of laser radiation was less than 0.15 nm. The pulse duration and the pulse-repetition rate of laser pulses were 7 ns and 10 Hz, respectively. The experiments were carried out at 80–320 K temperature range.

3. Results and Discussion

3.1. NPs Characterization (HR TEM, and X-Ray Diffraction). Transmission electron microscopy (TEM) data indicate that obtained Pr^{3+}:LaF_3 samples consist of nearly monodisperse well-crystallized NPs with an average diameter of 20 nm (Figure 1(a)). Also the sample has regular almost spherical shape. Selected area electron diffraction (SAED) patterns correspond to LaF_3 crystal structure (Figure 1(a)). The presence of circular rings in the SAED patterns indicates that the sample consists of disordered monocrystalline NPs. The lattice structures are clearly seen under the higher magnifications, what also confirms that each NP is monocrystalline (Figure 1(b)). According to the X-ray diffraction data (Figure 2), all the Pr:LaF_3 NPs were hexagonal structured crystals that correspond to the structure of matrixes of LaF_3 and PrF_3. Sharp peaks of the patterns also confirm good crystallinity of the NPs. The lack of amorphous phase was also proved. The diphenylamine test did not reveal presence of nitrates in the NPs colloidal solution after 4th stage of centrifugation. Those facts indicate that all the nitrate precursors and reaction products were removed and did not affect the physical properties of the samples.

3.2. Luminescent Nanothermometry of Pr^{3+}:LaF_3 (C_{Pr} = 1%) Crystal. Room-temperature luminescence spectra of Pr^{3+}:LaF_3 (C_{Pr} = 1%) microcrystalline powder and Pr^{3+}:LaF_3 (C_{Pr} = 12%) NPs excited by laser beam at 444 nm are presented in Figure 3. The spectra of Pr^{3+} ions for the powder and the NPs do not differ much between each other as it is commonly expected for rare-earth ions [28]. The luminescent spectra have the emissions bands at about 487, 523, 537, 580, 601, and 672 nm which are interpreted as a

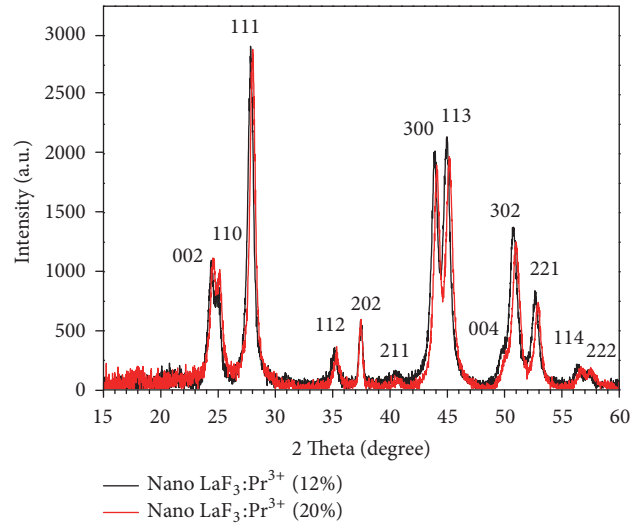

Figure 2: Experimental X-ray diffraction patterns of synthesized Pr^{3+}:LaF_3 nanoparticles.

result of the transition from the ^3P_j (j = 0, 1, 2) excited states to $^3H_4$, $^3H_5$, $^3H_6$, and $^3F_3$ states of Pr^{3+} ions, respectively [29]. The emission from $^1D_2$ state was not found under the excitation condition and at the studied temperature range. Probably the emission from $^1D_2$ is not observed because of the lack of nonradiative relaxation of ^3P_j to $^1D_2$ due to low cutoff phonon frequency in LaF_3 (350–400 cm^{-1}), which is 2 times less than one for YAG (700–865 cm^{-1}). Indeed to bridge the $^3P_0$–$^1D_2$ energy gap, the 9 phonons are required in case of LaF_3 and only 4 or 5 ones for YAG; thus, the multiphonon relaxation is expected negligible [21, 30]. Moreover, the electron phonon coupling constants of YAG are highly different from those of LaF_3 [21].

The temperature dependence of the luminescence spectra of the Pr^{3+}:LaF_3 microcrystalline powder is shown in Figure 4(a). The emission bands at about ~470–500, ~520–540, ~570–620, ~660–700, and ~690–730 nm corresponding to

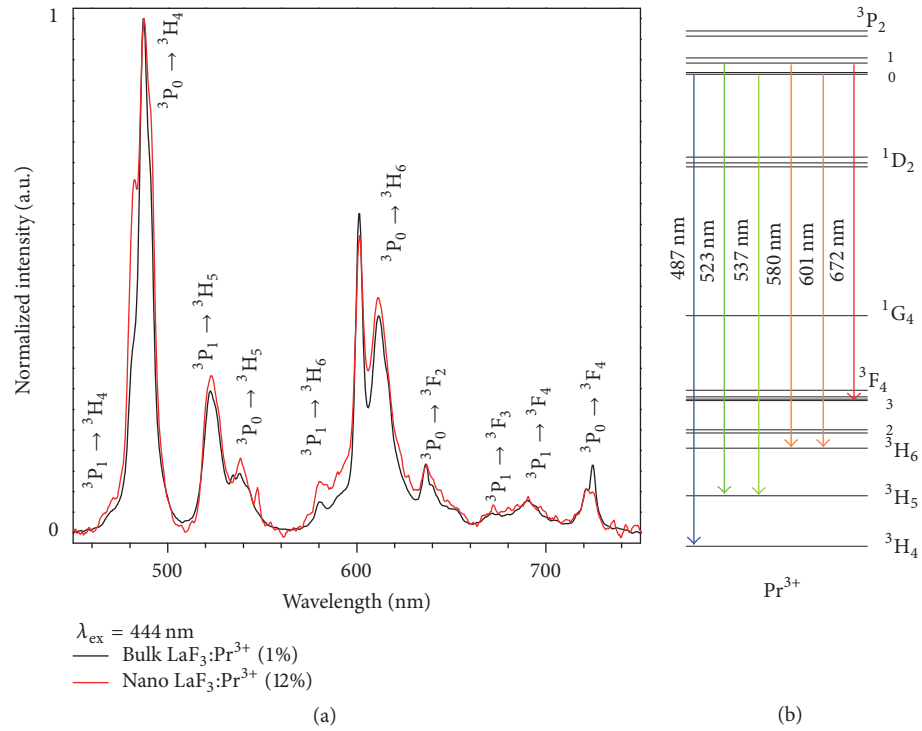

FIGURE 3: Emission spectrum of the Pr^{3+}:LaF_3 microcrystalline powder and the NPs under 444 nm excitation.

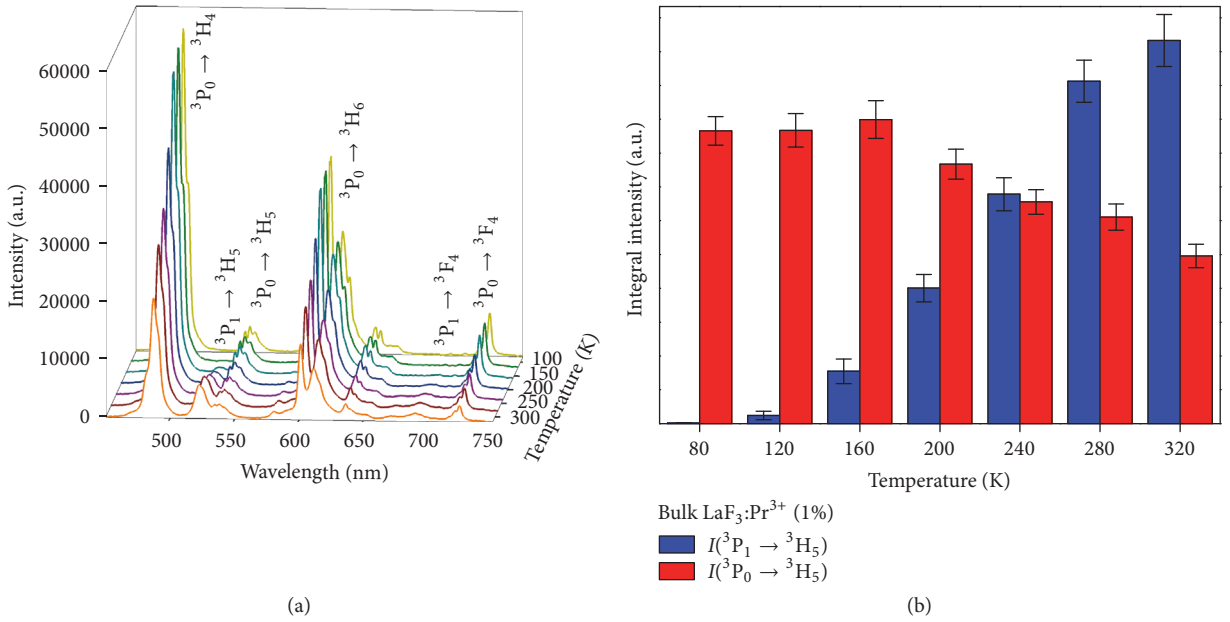

FIGURE 4: (a) Temperature dependent spectra of the Pr^{3+}:LaF_3 microcrystalline powder, recorded from 80 to 320 K under 444 nm excitation. (b) Histogram displaying the emission intensities of $^3P_0$ (~537 nm) and $^3P_1$ (~523 nm) levels at various temperatures.

the transitions from $^3P_1$ and $^3P_0$ to $^3H_4$, $^3H_5$, $^3H_6$, $^3F_3$, and $^3F_4$ states, respectively, are the most temperature sensitive in the range above 160 K. For instance, when the temperature increases from 80 to 160 K, both intensities of emissions from $^3P_0$ state (e.g., at ~487, ~537, ~610, and ~725 nm) and the ones from $^3P_1$ (e.g., at ~523 and about 660–700 nm) demonstrate negligible changes. And the intensities of luminescence from $^3P_1$ state were much less than from the $^3P_0$ one, whereas the emission from $^3P_0$ (at 487 nm) is decreased dramatically in contrast to the emission from $^3P_1$ (523 nm) which is increased

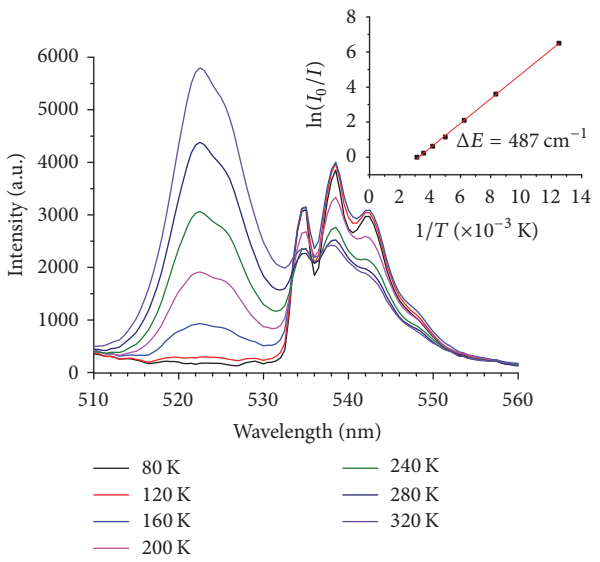

FIGURE 5: Temperature dependent spectra of the Pr^{3+}:LaF_3 microcrystalline powder for the emission intensities of $^3P_0$ (~537 nm) and $^3P_1$ (~523 nm) and the temperature dependence of $\ln(I/I_0)$ for ΔE calculation (inset).

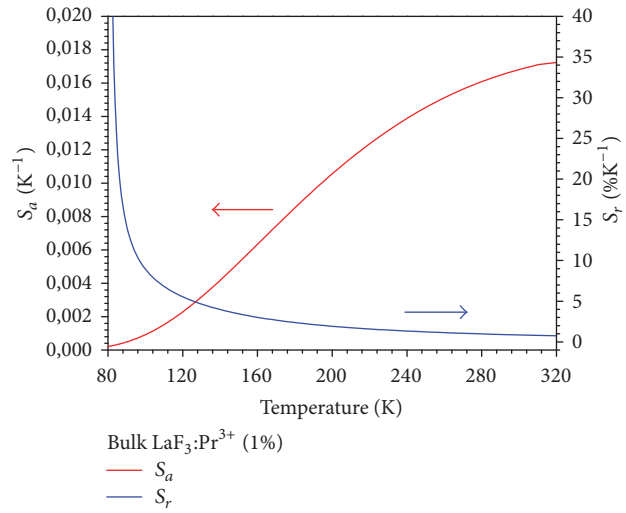

FIGURE 6: The absolute and relative sensitivities (S_a and S_r) of the Pr:LaF_3 microcrystalline powder as functions of the temperature under 444 nm excitation.

at the temperature higher than 160 K (Figure 4(a)). At the same time, the intensity of emission at about 537 nm from the same $^3P_0$ state stays almost constant into the temperature range from 80 to 160 K and decreases smoothly above 200 K probably because of overlapping spectral bands associated with the transitions from both $^3P_0$ and $^3P_1$ states as it is shown on the histogram (Figure 4(b)). Figure 5 also demonstrates temperature dependence of 523 and 532 nm emission bands. Generally, the temperature sensitivity looks similar to the process occurring in Pr^{3+}:β-$NaYF_4$ under excitation to $^3P_1$ state [31]: after excitation of $^3P_1$ state at 15 K, the nonradiative relaxation from $^3P_1$ to $^3P_0$ states takes place and the $^3P_0$-$^3H_4$ emission band is clearly observed. At 100 K, additional emission band appeared at 525 nm and 470 nm, which were assigned to transitions from $^3P_1$ state to $^3H_5$ and $^3H_4$ ones, respectively. In our case, decreasing of the intensity of the emission from $^3P_0$ (e.g., at about 487 nm or 537 nm) and simultaneous increasing of the intensity of the emission from $^3P_1$ (at 523 nm) at 80 K can be attributed to the fact that $^3P_1$ and $^3P_0$ states share their electronic populations according to the Boltzmann process [31]. It was shown in [31] that at 15 K the electrons remain in $^3P_0$ state, which is the only emitting state. Then, the thermalization of $^3P_1$ state begins at around 100 K and operates more and more efficiently upon warming [22, 31]. Also the intensity of the emission bands of rare-earth ions depends on several parameters among which, temperature is the most critical ones [1, 32] and transitions from $^3P_0$ are also temperature dependent. The relationship of the relative emission intensities with temperature can be used to calculate the activation energy (E_a) from thermal quenching using the following equation [33]:

$$\ln\left(\frac{I_0}{I}\right) = \ln A - \frac{E_a}{k_B T}, \quad (1)$$

where I_0 and I are the intensity of $^3P_1$ emission (at 523 nm) for the Pr^{3+}:LaF_3 microcrystalline powder at 80 K and the testing temperature (120–320 K), respectively (Figure 5). Here A is a constant, and k_B is the Boltzmann constant. The E_a and A were calculated to be $E_a = 487\,\text{cm}^{-1} \pm 40\,\text{cm}^{-1}$ and $A = -2{,}27058$. This value is in good agreement with value of the energy gap between $^3P_1$ and $^3P_0$ states which is about $500\,\text{cm}^{-1}$ [22]. The $\ln(I_0/I)$ as a function of temperature is shown on the inset of Figure 5. Therefore, the local temperature inside bulk crystal can be estimated by (1). The absolute and relative sensitivities (S_a and S_r) can be expressed by the following equations [6, 33, 34]:

$$S_a = \frac{1}{R}\frac{dR}{dT} = \frac{\Delta E}{k_B T^2}$$
$$S_r = \frac{dR}{dT} = R\left(\frac{\Delta E}{k_B T^2}\right), \quad (2)$$

where ΔE is the energy difference between thermally coupled levels, k_B is the Boltzmann constant, T is the absolute temperature, and R is the integrated luminescence ratio between the two thermally coupled levels $^3P_1$ and $^3P_0$. Noteworthy, the maximum value of S_a reaches $0.017\,\text{K}^{-1}$ (at 320 K), while the maximum value of S_r is 40% K^{-1} (at 443 K) (Figure 6). Figure 7 shows the ratio R between intensities of 537 and 523 nm emissions of Pr^{3+} ions as a function of temperature and the fitting is performed using calculated ΔE value. It is clearly seen that R rises from 0.01 to 2.3 (exhibiting a 200-time increase), as shown in Figure 6. These results indicate that the Pr^{3+}:LaF_3 (C_{Pr} = 1%) microcrystalline powder is a promising candidate for luminescent thermometry application especially in physiological temperature range (10–50°C).

3.3. Luminescent Nanothermometry of Pr^{3+}:LaF_3 (C_{Pr} = 12%, 20%) Nanoparticles. The intensity of luminescence of

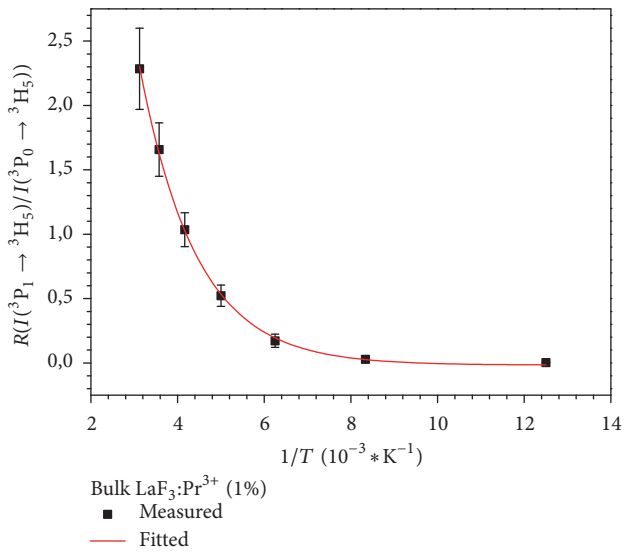

Figure 7: Ratio R between intensities of 537 and 523 nm emissions of Pr^{3+} ions as a function of temperature and the fitting is performed using calculated ΔE value.

the Pr^{3+}:LaF_3 NPs was at least one order of magnitude weaker than for the microcrystalline powder. The temperature dependent spectra of the Pr^{3+}:LaF_3 (C_{Pr} = 12% and 20%) NPs are shown in Figures 8(a) and 8(b), respectively. The intensities of two emission bands at about 487 and 538 nm corresponding to the $^3P_0$-$^3H_4$ and $^3P_0$-$^3H_5$ transitions, respectively, decrease significantly when the temperature rises from 80 to 320 K. Whereas unlike the Pr^{3+}:LaF_3 bulk crystal ones demonstrate drastic decrease only into the temperature range from 200 to 320 K. Also surprisingly, the Pr^{3+}:LaF_3 NPs luminescence at about 523 nm ($^3P_1$-$^3H_5$ transitions) demonstrates negligible intensity changing within the whole temperature range in contrast to the crystal bulk where it was most temperature dependent (see Figures 9(a) and 9(b)). To be fair, it should be noted that in case of Pr^{3+}:LaF_3 (C_{Pr} = 12%) NPs the emission band at 538 nm demonstrates slight increase of intensity from 80 K to 200 K and then remains almost constant within 240–320 K temperature range (Figure 9(a)). On the other hand, in case of Pr^{3+}:LaF_3 (C_{Pr} = 20%) NPs the emission peak at 538 nm remains constant within the whole temperature range (80–320 K). However, the emissions stipulated by transitions from $^3P_0$ state (e.g., at 487 and 538 nm) demonstrate significant change into the whole temperature range (80–320 K). It can be concluded that thermalization between $^3P_0$ and $^3P_1$ states dominates only for the Pr^{3+}:LaF_3 (C_{Pr} = 12%) NPs into the 80–200 K temperature range and another temperature dependent quenching mechanism of $^3P_0$ state takes place above 200 K. Indeed, the phonon spectrum of nanosized LaF_3 is modified and differs from the bulk one [28, 35]. This modified phonon spectrum can affect the interaction between $^3P_0$ and $^3P_1$ states. Besides, there are numerous other possible mechanisms that could affect luminescent transitions of rare-earth ions and which are dependent on the temperature: a multiphonon decay, an energy transfer between rare-earth ions or to quenching centers, appearance of phonon assisted Auger conversion processes, and thermal enhancement of energy transfer processes between rare-earth ions and the host levels or charge transfer states [1, 31, 32].

One of the significant differences between NPs and bulk crystals (including nanosized ones) is the increased role of surface and, as a consequence, interaction of ions with surface ligands [28]. It should be noted that the concentration of Pr^{3+} ions in the NPs is high; thus, concentration quenching takes place. This quenching can be related to migration of energy to quenching centers (most probably OH groups). This process is also temperature dependent for Pr^{3+} ions [36]. It is clearly seen from Figure 10 that S_a and S_r values for the NPs are almost two times less then ones for the crystal.

As it was mentioned above, the NPs were synthesized via coprecipitation method in water and the surface of the NPs probably covered with adsorbed OH groups [28]. Moreover, it is known that the NPs synthesized via the same method contain water clusters inside the structure [37]. Also, the slight inhomogeneity of the Pr^{3+}:LaF_3 (C_{Pr} = 12%) NPs structure shown on Figure 1(b) suggests the presence of water clusters inside the NPs. It means that there are two kinds of surfaces (internal and external) with adsorbed OH groups which can act as main quenching units attributed to nonradiative transitions from rare-earth exited state to a vibrational state of OH molecule [38, 39]. It is that the luminescence emission intensity of the NPs is less than ones for the crystal. As it is clearly seen from Figures 8(a) and 8(b), all the peaks corresponding to transitions from $^3P_0$ state strongly depend on temperature and, in contrast, the peaks corresponding to transitions from $^3P_1$ one do not demonstrate obvious temperature sensing properties. Therefore, in case of Pr^{3+}:LaF_3 NPs the temperature dependent nonradiative transitions from rare-earth $^3P_0$ exited state to a vibration state of OH groups dominate over the thermalization process and the populations of the excited $^3P_0$ and $^3P_1$ states decay quasi independently. The $^3P_1$ state lifetime is determined by rare-earth ions intracenter nonradioactive relaxation to $^3P_0$ state and that is why the correspondent emission intensities are weakly temperature sensitive. After analyzing the literature, several systems based on the rare-earth doped LaF_3 NPs operating in the physiological temperature range were chosen for the further comparison with the Pr^{3+} doped LaF_3 system. Also, temperature sensing technique of the chosen systems is based on the ratio of the fluorescence intensity of the emission bands corresponding to the suitable transitions. The value of relative temperature sensitivity for Pr^{3+}:LaF_3 macropowder and NPs (C_{Pr} = 12%, 20%) into the physiological temperature range at 45°C appeared to be 1.0, 0.5, and 0.3%°C^{-1}, respectively. The two well-known systems Nd^{3+}:LaF_3 (C_{Nd} = 10%) and Nd^{3+}, Yb^{3+}:LaF_3 (C_{Nd} = 10%, C_{Yb} = 10%) NPs demonstrate relative sensitivities around 0.01%°C^{-1} and 0.1%°C^{-1}, respectively [10, 11]. Also it should be noted that in case of Dy^{3+}:LaF_3 transparent glass ceramics [6], Nd^{3+}:LaF_3 (C_{Nd} = 10%) and Nd^{3+}, Yb^{3+}:LaF_3 (C_{Nd} = 10%, C_{Yb} = 10%) NPs [10, 11], and our systems the relative sensitivity curves decay almost linearly in the physiological temperature range. Probably, in order to increase relative

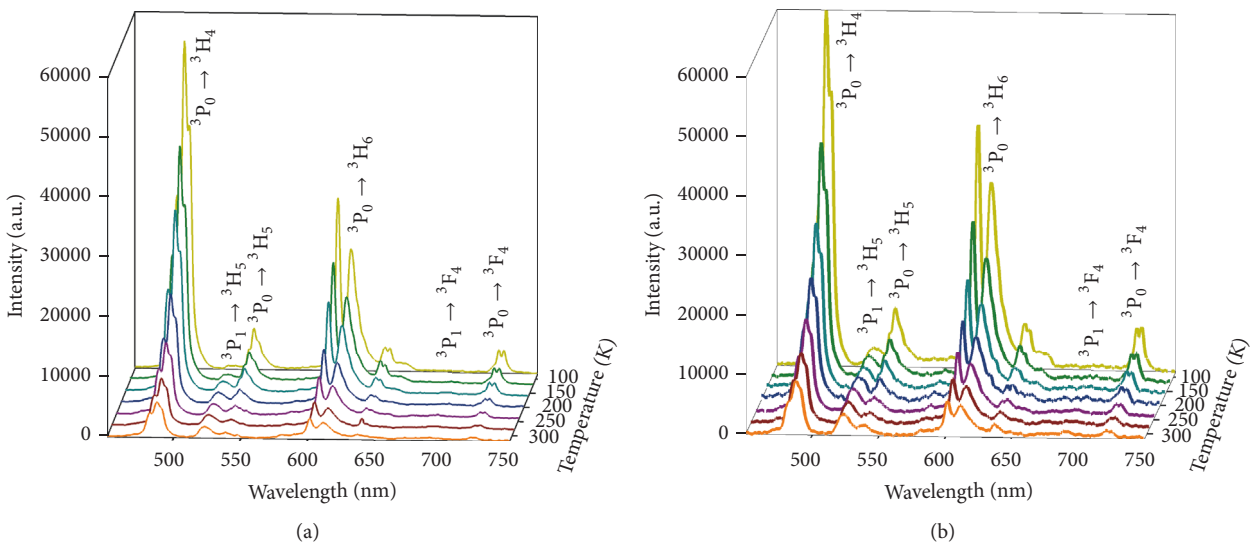

FIGURE 8: Temperature dependent spectra of the Pr:LaF_3 (C_{Pr} = 12%) (a), (C_{Pr} = 20% (b)) NPs, recorded from 80 to 320 K under 444 nm excitation.

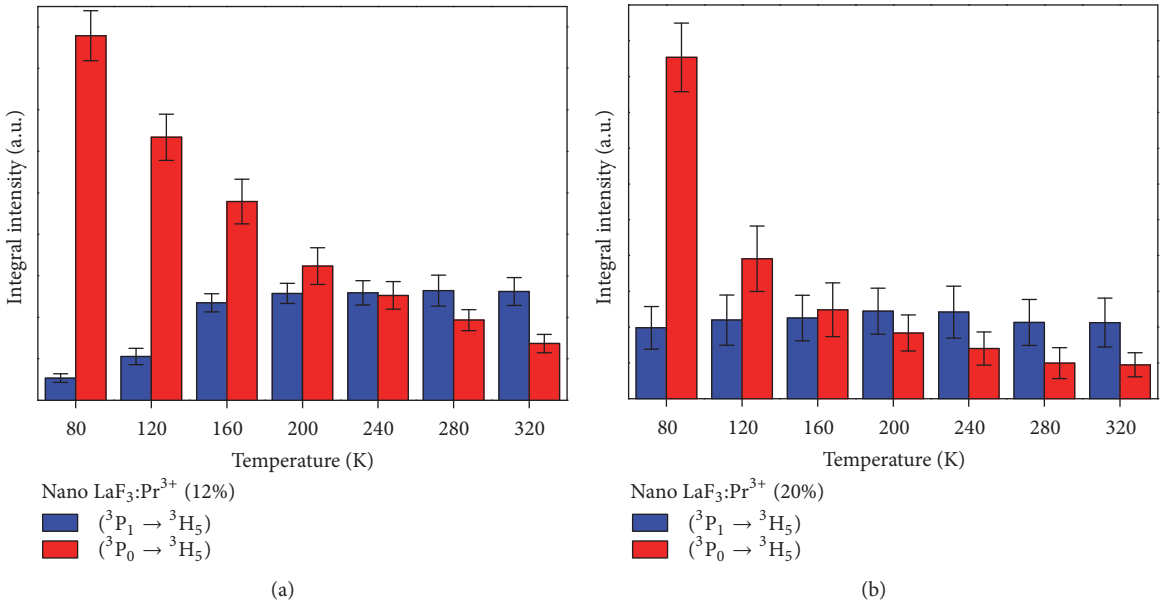

FIGURE 9: Histogram displaying the emission intensities of $^3P_0$ (~537 nm) and $^3P_1$ (~523 nm) levels at various temperatures of the Pr:LaF_3 (C_{Pr} = 12% (a), (C_{Pr} = 20% (b)) NPs.

sensitivity of Pr^{3+}:LaF_3 NPs, the concentration of Pr^{3+} ions in LaF_3 host matrix should be reduced and addition experiment should be carried out in the future.

The thermometer performance is characterized not only by the relative sensitivity but also by the maximum temperature uncertainty. The minimum temperature uncertainty can be estimated using

$$\delta T = \frac{1}{S_r}\frac{\delta D}{D}, \tag{3}$$

where $\delta D/D$ is the relative uncertainty in the determination of the thermometric parameter (we use the typical $\delta D/D$ value of a portable detector, 0.5%) [40]. The temperature uncertainty in the physiological temperature range for Pr^{3+}:LaF_3 macropowder and NPs (C_{Pr} = 12%, 20%) was 0.5, 1.0, and 1.7°C. These values are comparable with Yb^{3+}/Er^3+-doped PbF_2 nanocrystal as temperature sensor (δT = 1/0°C). The technique presents temperature uncertainty 1.0 K. Also, the repeatability of a thermometer's readout upon temperature cycling is quantified using the expression [41]:

$$R = 1 - \frac{\max\left(\left|\Delta_c - \Delta_i\right|\right)}{\Delta_c}. \tag{4}$$

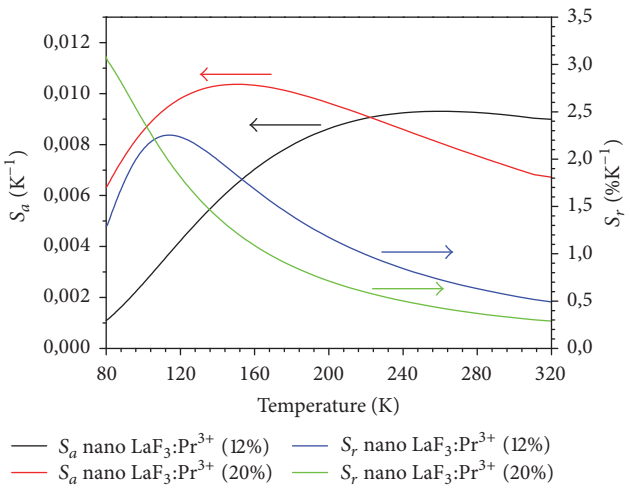

FIGURE 10: The absolute and relative sensitivities (S_a and S_r) of the Pr^{3+}:LaF_3 (C_{Pr} = 12% (a), (C_{Pr} = 20% (b)) NPs as functions of the temperature under 444 nm excitation.

Thermometric parameter is recorded in 10 heating-cooling temperature cycles showing reproducibility higher than 99.1% for all the samples (Pr^{3+}:LaF_3 macropowder, and NPs (C_{Pr} = 12%, 20%)).

4. Conclusion

In summary, the Pr^{3+} ions doped LaF_3 crystal and NPs were demonstrated to be one of the most promising inorganic optical temperature sensing materials in the temperature range from 80 to 320 K, including physiological temperature range (10–50°C). The NPs are nontoxic at micromolar concentrations [22], which is extremely important for biomedical application. The two thermal sensing peaks at 690 nm and 723 nm corresponding to $^3P_1$-$^3F_4$ and $^3P_0$- $^3F_4$ transitions, respectively, situated within the biological window open the way for subtissue thermal sensing. The absolute and relative sensitivities (S_a and S_r) reach values of 0.017 K^{-1} (at 320 K) and 40% K^{-1} (at 443 K), respectively.

It was revealed that the mechanisms of temperature sensitivity for the crystal and the NPs are different. In the crystal, the $^3P_1$ and $^3P_0$ states share their electronic populations according to the Boltzmann and thermalization of $^3P_1$ state takes place. In the NPs, there are two temperature dependent mechanisms: energy migration within $^3P_0$ state in the temperature range from 80 K to 200 K followed by quenching of $^3P_0$ state by OH groups at temperatures higher 200 K. The latter process dominates over the thermalization between $^3P_0$ and $^3P_1$ states. It is also demonstrated that S_r of the NPs increases when the concentration of Pr^{3+} ions decreases and can be optimized by choosing suitable concentration of Pr^{3+} ions. For example, the value of relative temperature sensitivity for Pr^{3+}:LaF_3 macropowder and NPs (C_{Pr} = 12%, 20%) into the physiological temperature range appeared to be 1.0, 0.5, and 0.3%°C^{-1}, respectively.

Conflicts of Interest

The authors declare that they have no conflicts of interest.

Acknowledgments

Microscopy studies were carried out at the Interdisciplinary Center of Analytical Microscopy of Kazan Federal University. The microscopy studies were funded by the subsidy of the Russian Government [Agreement no. 02.A03.21.0002] to support the Program of Competitive Growth of Kazan Federal University among World's Leading Academic Centers. The synthesis of the nanoparticles, crystal growth, and X-ray diffraction experiments were supported by the Russian Foundation of Basic Research (RFBR) Grant no. 15-02-08648 A and the optical spectroscopy experiments were supported by the state assignment in the sphere of scientific activities (Project no. 3.1156.2017/4.6).

References

[1] D. Jaque and F. Vetrone, "Luminescence nanothermometry," *Nanoscale*, vol. 4, no. 15, pp. 4301–4326, 2012.

[2] G. P. Szakmany, A. O. Orlov, G. H. Bernstein, and W. Porod, "Single-metal nanoscale thermocouples," *IEEE Transactions on Nanotechnology*, vol. 13, no. 6, pp. 1234–1239, 2014.

[3] J. P. Kauppinen and J. P. Pekola, "Coulomb blockade nanothermometer," *Microelectronic Engineering*, vol. 41-42, pp. 503–506, 1998.

[4] C. D. S. Brites, P. P. Lima, N. J. O. Silva et al., "Thermometry at the nanoscale," *Nanoscale*, vol. 4, no. 16, pp. 4799–4829, 2012.

[5] X.-D. Wang, O. S. Wolfbeis, and R. J. Meier, "Luminescent probes and sensors for temperature," *Chemical Society Reviews*, vol. 42, no. 19, pp. 7834–7869, 2013.

[6] Y. Y. Bu, S. J. Cheng, X. F. Wang, and X. H. Yan, "Optical thermometry based on luminescence behavior of Dy3+-doped transparent LaF3 glass ceramics," *Applied Physics A*, vol. 121, no. 3, pp. 1171–1178, 2015.

[7] G. Tessier, M. Bardoux, C. Boú, C. Filloy, and D. Fournier, "Back side thermal imaging of integrated circuits at high spatial resolution," *Applied Physics Letters*, vol. 90, no. 17, 2007.

[8] B. Dong, B. Cao, Y. He, Z. Liu, Z. Li, and Z. Feng, "Temperature sensing and in vivo imaging by molybdenum sensitized visible upconversion luminescence of rare-earth oxides," *Advanced Materials*, vol. 24, no. 15, pp. 1987–1993, 2012.

[9] E. C. Ximendes, U. Rocha, K. U. Kumar, C. Jacinto, and D. Jaque, "LaF3 core/shell nanoparticles for subcutaneous heating and thermal sensing in the second biological-window," *Applied Physics Letters*, vol. 108, no. 25, 2016.

[10] U. Rocha, C. Jacinto Da Silva, W. Ferreira Silva et al., "Subtissue thermal sensing based on neodymium-doped LaF3 nanoparticles," *ACS Nano*, vol. 7, no. 2, pp. 1188–1199, 2013.

[11] E. C. Ximendes, W. Q. Santos, U. Rocha et al., "Unveiling in vivo subcutaneous thermal dynamics by infrared luminescent nanothermometers," *Nano Letters*, vol. 16, no. 3, pp. 1695–1703, 2016.

[12] Y. Gao, F. Huang, H. Lin, J. Xu, and Y. Wang, "Intervalence charge transfer state interfered Pr^{3+} luminescence: a novel strategy for high sensitive optical thermometry," *Sensors and Actuators, B: Chemical*, vol. 243, pp. 137–143, 2017.

[13] X. Rao, T. Song, J. Gao et al., "A highly sensitive mixed lanthanide metal-organic framework self-calibrated luminescent thermometer," *Journal of the American Chemical Society*, vol. 135, no. 41, pp. 15559–15564, 2013.

[14] H. Dong, S.-R. Du, X.-Y. Zheng et al., "Lanthanide nanoparticles: from design toward bioimaging and therapy," *Chemical Reviews*, vol. 115, no. 19, pp. 10725–10815, 2015.

[15] A. B. Shcherbakov, N. M. Zholobak, A. E. Baranchikov, A. V. Ryabova, and V. K. Ivanov, "Cerium fluoride nanoparticles protect cells against oxidative stress," *Materials Science and Engineering C*, vol. 50, pp. 151–159, 2015.

[16] M. L. Debasu, D. Ananias, I. Pastoriza-Santos, L. M. Liz-Marzán, J. Rocha, and L. D. Carlos, "All-in-one optical heater-thermometer nanoplatform operative from 300 to 2000 K based on Er3+ emission and blackbody radiation," *Advanced Materials*, vol. 25, no. 35, pp. 4868–4874, 2013.

[17] M. D. Dramićanin, Ž. Antić, S. Ćulubrk, S. P. Ahrenkiel, and J. M. Nedeljković, "Self-referenced luminescence thermometry with Sm3+ doped TiO2 nanoparticles," *Nanotechnology*, vol. 25, no. 48, 2014.

[18] U. Rocha, K. U. Kumar, C. Jacinto et al., "Nd^{3+} doped LaF_3 nanoparticles as self-monitored photo-thermal agents," *Applied Physics Letters*, vol. 104, no. 5, 2014.

[19] V. K. Rai, D. K. Rai, and S. B. Rai, "Pr 3+ doped lithium tellurite glass as a temperature sensor," *Sensors and Actuators, A: Physical*, vol. 128, no. 1, pp. 14–17, 2006.

[20] M. Kaczkan, Z. Boruc, B. Fetlinski, S. Turczynski, and M. Malinowski, "Temperature dependence of 3P0 Pr3+ fluorescence dynamics in Y4Al2O9 crystals," *Applied Physics B: Lasers and Optics*, vol. 113, no. 2, pp. 277–283, 2013.

[21] I. Kamma, P. Kommidi, and B. R. Reddy, "High temperature measurement using luminescence of Pr^{3+} doped YAG and Ho^{3+} doped CaF_2," *Physica Status Solidi (C) Current Topics in Solid State Physics*, vol. 6, no. 1, pp. S187–S190, 2009.

[22] Y. An, A. Duhaime, and P. S. May, "Optical observation of the kinetics of thermalization between the $^3P_0$ and $^3P_1$ excited states of Pr^{3+} in symmetrical Pr^{3+}-Gd^{3+} pairs in $CsCdBr_3$," *Journal of Luminescence*, vol. 111, no. 3, pp. 131–138, 2005.

[23] E. Cavalli, P. Boutinaud, and M. Grinberg, "Luminescence dynamics in CaWO4:Pr3+ powders and single crystals," *Journal of Luminescence*, vol. 169, pp. 450–453, 2016.

[24] M. S. Pudovkin, P. V. Zelenikhin, A. O. Krasheninnikova et al., "Photoinduced toxicity of PrF3 and LaF3 nanoparticles," *Optics and Spectroscopy*, vol. 121, no. 4, pp. 538–543, 2016.

[25] E. M. Alakshin, A. V. Klochkov, E. I. Kondratyeva et al., "Microwave-assisted hydrothermal synthesis and annealing of DyF_3 nanoparticles," *Journal of Nanomaterials*, vol. 2016, Article ID 7148307, 5 pages, 2016.

[26] E. M. Alakshin, R. R. Gazizulin, A. V. Klochkov et al., "Annealing of PrF_3 nanoparticles by microwave irradiation," *Optics and Spectroscopy*, vol. 116, no. 5, pp. 721–723, 2014.

[27] O. A. Morozov, A. K. Naumov, A. V. Lovchev, and E. Y. Tselishcheva, "Up-conversion luminescence of LaF3:Pr3+ crystal," *Journal of Physics: Conference Series*, vol. 560, no. 1, article 012012, 2014.

[28] S. P. Feofilov, "Spectroscopy of dielectric nanocrystals doped by rare-earth and transition-metal ions," *Physics of the Solid State*, vol. 44, no. 8, pp. 1407–1414, 2002.

[29] H. Okamoto, K. Kasuga, I. Hara, and Y. Kubota, "Visible-NIR tunable Pr3+-doped fiber laser pumped by a GaN laser diode," *Optics Express*, vol. 17, no. 22, pp. 20227–20232, 2009.

[30] J. W. Stouwdam, G. A. Hebbink, J. Huskens, and F. C. J. M. van Veggel, "Lanthanide-doped nanoparticles with excellent luminescent properties in organic media," *Chemistry of Materials*, vol. 15, no. 24, pp. 4604–4616, 2003.

[31] P. Boutinaud, R. Mahiou, N. Martin, and M. Malinowski, "Luminescence from Pr3+3P1 and 3P2 states in β-NaYF4: Pr3+," *Journal of Luminescence*, vol. 72-74, pp. 809–811, 1997.

[32] G. F. Imbusch and B. Henderson, *Optical Spectroscopy of Inorganic Solids*, Oxford Science Publications, London, UK, 2006.

[33] C.-H. Huang, L. Luo, Y.-T. Yeh, S.-M. Jang, and W.-R. Liu, "Novel red-emitting garnet Na2CaTi2Ge 3O12:Pr3+,Na+ phosphors," *RSC Advances*, vol. 4, no. 11, pp. 5513–5517, 2014.

[34] H. Suo, C. Guo, and T. Li, "Broad-scope thermometry based on dual-color modulation up-conversion phosphor Ba5Gd8Zn4O21:Er3+/Yb3+," *Journal of Physical Chemistry C*, vol. 120, no. 5, pp. 2914–2924, 2016.

[35] H.-S. Yang, K. S. Hong, S. P. Feofilov, B. M. Tissue, R. S. Meltzer, and W. M. Dennis, "Electron-phonon interaction in rare earth doped nanocrystals," *Journal of Luminescence*, vol. 83-84, pp. 139–145, 1999.

[36] P. M. Selzer, D. S. Hamilton, R. Flach, and W. M. Yen, "Phonon-assisted energy migration in Pr3+ : LaF3," *Journal of Luminescence*, vol. 12-13, no. C, pp. 737–741, 1976.

[37] E. M. Alakshin, D. S. Blokhin, A. M. Sabitova et al., "Experimental proof of the existence of water clusters in fullerene-like PrF_3 nanoparticles," *JETP Letters*, vol. 96, no. 3, pp. 181–183, 2012.

[38] K. Ramasesha, L. De Marco, A. Mandal, and A. Tokmakoff, "Water vibrations have strongly mixed intra- and intermolecular character," *Nature Chemistry*, vol. 5, no. 11, pp. 935–940, 2013.

[39] J. K. Krebs, S. P. Feofilov, A. A. Kaplyanskii, R. I. Zakharchenya, and U. Happek, "Non-radiative relaxation of Yb3+ in highly porous γ-Al2O3," *Journal of Luminescence*, vol. 83-84, pp. 209–213, 1999.

[40] M. Ren, C. D. S. Brites, S.-S. Bao, R. A. S. Ferreira, L.-M. Zheng, and L. D. Carlos, "A cryogenic luminescent ratiometric thermometer based on a lanthanide phosphonate dimer," *Journal of Materials Chemistry C*, vol. 3, no. 33, pp. 8480–8484, 2015.

[41] C. D. S. Brites, A. Millán, and L. D. Carlos, "Lanthanides in luminescent thermometry," in *Handbook on the Physics and Chemistry of Rare Earths*, vol. 49, pp. 339–427, 2016.